Inorganic Chemistry

pubs.acs.org/IC

Article

Synthesis and Dynamics of Ferrous Polychalcogenides $[Fe(E_x)(CN)_2(CO)_2]^{2-}$ (E = S, Se, or Te)

Yu Zhang, Toby Woods, and Thomas B. Rauchfuss*

Cite This: *Inorg. Chem.* 2022, 61, 8241−8249

Read Online

ACCESS | Metrics & More | Article Recommendations | Supporting Information

ABSTRACT: Elemental chalcogens react with $[Fe(CN)_2(CO)_3]^{2-}$ to give the following ferrous derivatives: $[K(18\text{-crown-6})]_2[Fe(S_5)(CN)_2(CO)_2]$, $[K(18\text{-crown-6})]_2[Fe(S_2)(CN)_2(CO)_2]$, $[K(18\text{-crown-6})]_2[Fe(Se_4)(CN)_2(CO)_2]$, $[K(18\text{-crown-6})]_2[Fe(Te_2)(CN)_2(CO)_2]$, and $(NEt_4)_2[Fe(Te_2)(CN)_2(CO)_2]$. While these complex anions crystallized in a single stereochemistry (i.e., *trans* dicyanides or *cis* dicyanides), they isomerize in solution upon irradiation. The results are benchmarked by the corresponding studies on benzyl thiolate $[K(18\text{-crown-6})]_2[Fe(SBn)_2(CN)_2(CO)_2]$.

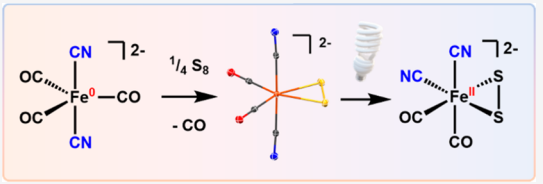

INTRODUCTION

Given the pervasiveness and importance of iron sulfides in nature,[1] one might expect that the chemistry of iron polysulfides would be well developed. The situation is, however, otherwise. The inventory of iron polysulfides includes only tetrahedral pentasulfido complexes $[Fe_2(\mu\text{-}S)_2(S_2)_2]^{2-}$,[2] $[S_2M(\mu\text{-}S)_2FeS_2]^{2-}$ (M = Mo or W),[3] and $[(NO)_2FeS_2]^-$.[4] A few iron clusters are known with bridging S_4 groups.[5] Octahedral iron polysulfido complexes have not been reported. This project addresses this gap. A further incentive is our search for new platform complexes that might be useful in elucidating the biochemistry of Fe−CN−CO−S complexes, which are related to the biosynthesis of the [FeFe]-hydrogenases[6−9] as well as the artificial maturation[10] of the [NiFe]-hydrogenases.[11] A well-characterized Fe−S_x−CO−CN complex is $[Fe_2(\mu\text{-}S_2)(CN)(CO)_5]^-$, which we recently prepared from $Fe_2(\mu\text{-}S_2)(CO)_6$.[12]

This paper focuses on the oxidative addition of S−S bonds to $[Fe(CN)_2(CO)_3]^{2-}$.[13] This Fe(0) precursor complex is known to be susceptible to oxidative addition, e.g., by H^+ and Me^+.[14] The work was extended to include the heavier chalcogens. The new polychalcogenide complexes are amenable to analysis of the nuclear magnetic resonance (NMR) spectroscopic signatures of the ancillary ligands, which provide insights into the synthetic pathways and dynamics. Previous mechanistic studies of the oxidative addition of the elemental chalcogens are rare. For example, the premier polysulfide complex with NMR-responsive ancillary ligands is Cp_2TiS_5.[15] It does not equilibrate with other polysulfido complexes, and its chemical evolution on the synthetic time scale remains unclear.

Finally, iron polysulfides are potentially relevant to two topical themes: batteries and the chemistry of evolution.[16,17]

RESULTS AND DISCUSSION

$[K(18\text{-crown-6})]_2[Fe(S_5)(CN)_2(CO)_2]$. Addition of 1 equiv of S_8 to a solution of $[K(18\text{-crown-6})]_2[Fe(CN)_2(CO)_3]$ led to a dark orange solution. The color lightens over the course of hours as the sulfur dissolves. The reaction also generates carbon monoxide as indicated by gas chromatographic analysis of the headspace. Orange microcrystals of $[K(18\text{-crown-6})]_2[Fe(S_5)(CN)_2(CO)_2]$ ($[K(18\text{-crown-6})]_2[\mathbf{FeS_5}]$) were obtained in 56% yield after workup (Scheme 1). Solutions of this salt appear to be stable under air for hours at room temperature if protected from light.

Scheme 1. Synthesis of $[Fe(S_5)(CN)_2(CO)_2]^{2-}$

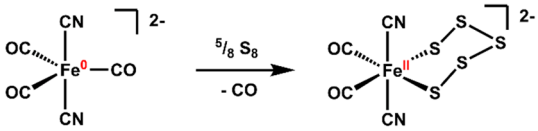

The structure of this salt was verified by X-ray crystallography (Figure 1). The Fe(II) center is octahedral. Of the three geometric isomers that are possible for Fe(chel)X_2Y_2 (chel = chelating ligands), only the achiral *trans*-dicyanide diastereomer *cis,trans,cis*-$[Fe(S_5)(CN)_2(CO)_2]^{2-}$ is observed in the solid state. The pentasulfido ligand adopts the chair conformation, which renders the CN ligands nonequivalent (see below). Each $[K(18\text{-crown-6})]^+$ center interacts with one Fe*C*N group, and additionally, one of the $[K(18\text{-crown-6})]^+$

Received: February 28, 2022
Published: May 13, 2022

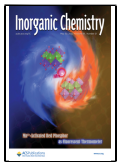

https://doi.org/10.1021/acs.inorgchem.2c00684
Inorg. Chem. 2022, 61, 8241−8249

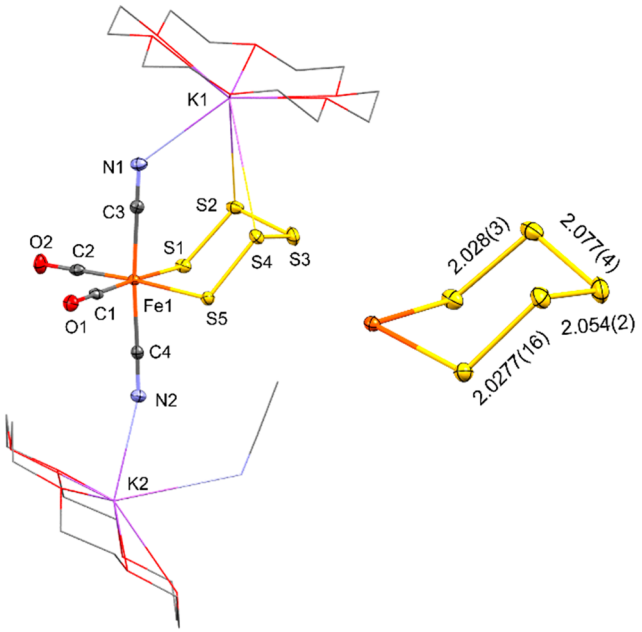

Figure 1. Structure of the $[K(18\text{-crown-6})]_2[Fe(S_5)(CN)_2(CO)_2]\cdot$MeCN. Hydrogen atoms have been omitted for the sake of clarity. Selected distances (angstroms): Fe(1)−C(1), 1.782(5); Fe(1)−C(2), 1.785(5); Fe(1)−C(3), 1.936(4); Fe(1)−C(4), 1.938(4); Fe(1)−S(1), 2.3623(12); Fe(1)−S(5), 2.3578(13).

centers interacts with two sulfane atoms in the FeS_5 ring, resulting in nine-coordinate K^+. The weakness of the K···S bonds is indicated by long K···S distances: K(1)−S(2) [3.630(3) Å] and K(1)−S(4) [3.7354(16) Å]. In [K(18-crown-6)][$(NO)_2FeS_5$], the potassium cation interacts with both coordinated S atoms [$d_{(K\cdots S)avg}$ = 3.610 Å].[18]

Monitoring the reaction of $[K(18\text{-crown-6})]_2[Fe(^{13}CN)_2(CO)_3]$ with 1 equiv of S_8 by ^{13}C NMR spectroscopy and ESI mass spectrometry (ESI-MS) revealed that several products are produced (Figures S34 and S35). These species likely correspond to the tetra-, hexa-, and heptasulfides $([Fe(S_x)(CN)_2(CO)_2]^{2-}$ (x = 4, 6, and 7, respectively). Recrystallization of this mixture gave samples that are ∼90% of the *cis,trans,cis*-pentasulfide.

The Fourier-transform infrared (FT-IR) spectrum of $[K(18\text{-crown-6})]_2[Fe(S_5)(CN)_2(CO)_2]$ in an acetonitrile solution features ν_{CO} bands at 2013 and 1956 cm^{-1} (Figure 2). The oxidation of Fe(0) by S_8 is indicated by the 141 cm^{-1} shift in ν_{COavg} to 1985 cm^{-1} from 1844 cm^{-1} for $[Fe(CN)_2(CO)_3]^{2-}$. Weaker bands at 2108 and 2094 cm^{-1} are assigned to ν_{CN} modes. The salt is soluble in water, which is unusual for a metal polysulfido complex. The IR bands in the ν_{CO} region are significantly shifted to a higher energy for solutions in MeOH and H_2O versus MeCN (Figure 2). Although anionic Fe*CN* centers are well-known to engage in hydrogen bonding,[19−21] simple explanations for the solvent-dependent ν_{CO} and ν_{CO} band are complicated by the likely disruption of FeCN···K and FeS···K interactions by these highly polar solvents.

The ^{13}CN NMR signal assigned to *cis,trans,cis*-$\mathbf{FeS_5}$ is broad at room temperature, which is due to a dynamic process. To further probe the solution behavior, we examined $[Fe(S_5)(^{13}CN)_2(CO)_2]^{2-}$ ($[^{13}\mathbf{FeS_5}]^{2-}$) by ^{13}C NMR spectroscopy (Figure 3A). At −60 °C, the ^{13}CN signals are split into doublets at δ 157.6 and 153.4 with a J of 10.6 Hz (a rare case for observing *trans*-$M(CN)_2$ coupling). Line shape analyses

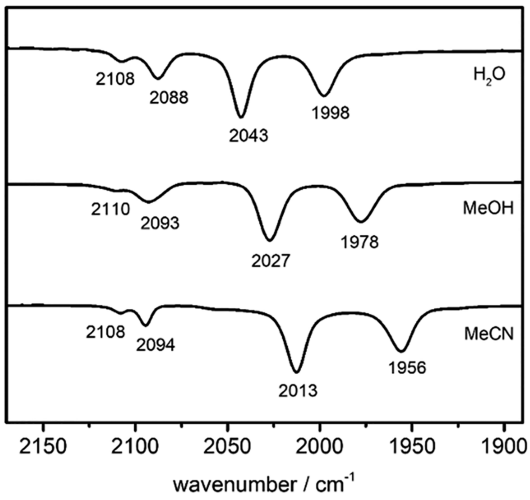

Figure 2. FT-IR spectrum of $[K(18\text{-crown-6})]_2[Fe(S_5)(CN)_2(CO)_2]$ in various solvents.

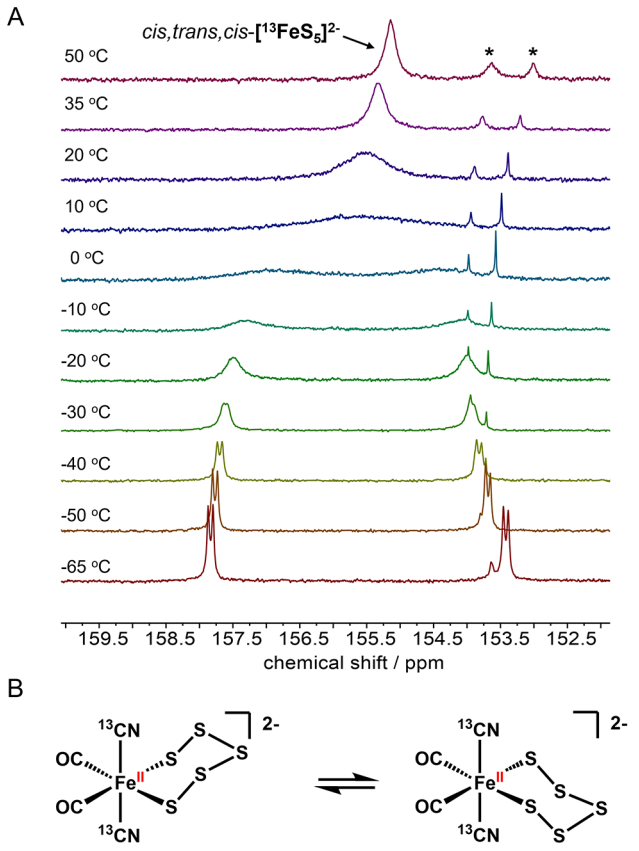

Figure 3. (A) ^{13}C NMR spectra (cyanide region) at various temperatures for a CD_3OD solution of $[K(18\text{-crown-6})]_2[Fe_2(S_5)(^{13}CN)_2(CO)_2]$. Asterisks correspond to unidentified species. (B) Proposed dynamic process for $[Fe_2(S_5)(^{13}CN)_2(CO)_2]^{2-}$.

were performed to extract rate constants at temperatures between 223 and 263 K. Eyring analyses afforded the following activation parameters: $\Delta H^{\ddagger}$ = 12.74 (0.33) kcal/mol, $\Delta S^{\ddagger}$ = 0.66 (1.39) cal K^{-1} mol^{-1}, and $\Delta G^{\ddagger}$(298 K) = 12.9 kcal/mol for $[^{13}\mathbf{FeS_5}]^{2-}$. Details of the analyses are provided in the Supporting Information. The small entropy change between initial and transition states indicates an intramolecular process

https://doi.org/10.1021/acs.inorgchem.2c00684
Inorg. Chem. 2022, 61, 8241−8249

(Figure 3B), which is consistent with a polysulfide ring flipping process as also seen in Cp_2TiS_5.[22]

Solutions (CD_3OD) of $[K(18\text{-crown-}6)]_2[Fe(S_5)(^{13}CN)_2(CO)_2]$ are light-sensitive. The ESI-MS analysis of samples exposed to ambient light shows ion currents for $\{K[Fe(S_x)(^{13}CN)_2(CO)_y]\}^-$ (x = 4, 5, 6, or 7; y = 0 or 2), whereas the freshly prepared samples show only signals for the S_5 complex (Figures S31 and S33). ^{13}C NMR spectra of photolyzed samples also show three pairs of ^{13}CN doublets, implicating *cis,cis,cis* isomers of $[Fe(S_x)(^{13}CN)_2(CO)_2]^{2-}$ [x = 4−7 (Figure S32)]. Additionally, a small amount of $S^{13}CN^-$ ($\delta_{S^{13}CN}$ = 133.5) and black solids were observed. Thus, the overall photochemical process is complex, involving changes in both polysulfane ring size and geometry.

$[K(18\text{-crown-}6)]_2[Fe(S_2)(CN)_2(CO)_2]$. Methanol solutions of $[K(18\text{-crown-}6)]_2[FeS_5]$ react with PPh_3 to generate solutions containing $SPPh_3$, as verified by ^{31}P NMR spectroscopy. This result implies the existence of low-S/Fe ratio derivatives. Indeed, treatment of $[K(18\text{-crown-}6)]_2[Fe(CN)_2(CO)_3]$ with 0.25 equiv of S_8 gave $[K(18\text{-crown-}6)]_2[Fe(S_2)(CN)_2(CO)_2]$ ($[K(18\text{-crown-}6)]_2[\mathbf{FeS_2}]$), which could be crystallized in moderate yield (Scheme 2). X-ray

Scheme 2. Synthesis of $[Fe(S_2)(CN)_2(CO)_2]^{2-}$

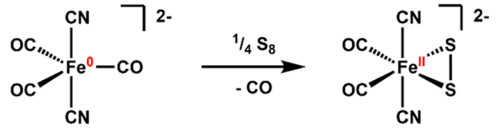

crystallography revealed the *cis,trans,cis* isomer with C_{2v} point group symmetry. As seen throughout this work, the $[K(18\text{-crown-}6)]^+$ centers are weakly associated with the cyanide and chalcogen ligands (Figure 4A). Monomeric iron persulfides have not been previously reported.

The ^{13}C NMR spectrum (Figure S6) of $[\mathbf{FeS_2}]^{2-}$ features three sets of CO and CN signals; the major pair (δ_{CO} = 216.6, δ_{CN} = 155.4) is assigned to the stereoisomer that was characterized by X-ray crystallography, i.e., *trans* cyanides and *cis* carbonyls (see below). The two minor pairs of ^{13}C NMR signals, being equal in intensity, are assigned to the all-*cis* isomer. The ratio of two isomers is 5:2. To further verify the solution speciation, we prepared the ^{13}CN-labeled $[K(18\text{-crown-}6)]_2[Fe(S_2)(^{13}CN)_2(CO)_2]$ ($[^{13}\mathbf{FeS_2}]^{2-}$). It was expected that two chemically inequivalent CN ligands in the all-*cis* isomer will exhibit two mutually coupled doublets in the ^{13}C NMR spectrum. Indeed, the cyanide singlets for the minor species in $[^{12}\mathbf{FeS_2}]^{2-}$ split into doublets in $[^{13}\mathbf{FeS_2}]^{2-}$ with a $^2J_{CC}$ of 13.2 Hz.

Ambient light readily induces isomerization of $[^{13}\mathbf{FeS_2}]^{2-}$. In a CD_3OD solution, the isomer ratio changes from ∼6:1 to ∼1:3 (*cis,trans,cis*:*cis,cis,cis*) over the course of ∼1 h (Figure 5).

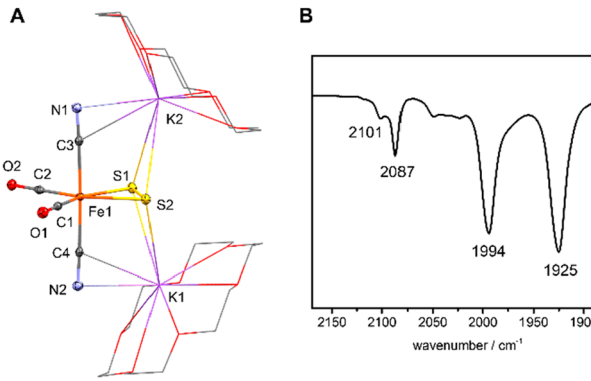

Figure 4. (A) Structure of $[K(18\text{-crown-}6)]_2[Fe(S_2)(CN)_2(CO)_2]$. Hydrogen atoms have been omitted for the sake of clarity. Selected distances (angstroms): Fe(1)−C(1), 1.763(2); Fe(1)−C(2), 1.765(2); Fe(1)−C(3), 1.933(2); Fe(1)−C(4), 1.940(2); Fe(1)−S(1), 2.3167(6); Fe(1)−S(2), 2.3163(5); S(1)−S(2), 2.0526(7); K(1)−S(2), 3.5013(6); K(1)−S(1), 3.5311(7); K(2)−S(1), 3.4447(7); K(2)−S(2), 3.4691(7). (B) FT-IR spectrum of $[K(18\text{-crown-}6)]_2[Fe(S_2)(CN)_2(CO)_2]$ in MeCN.

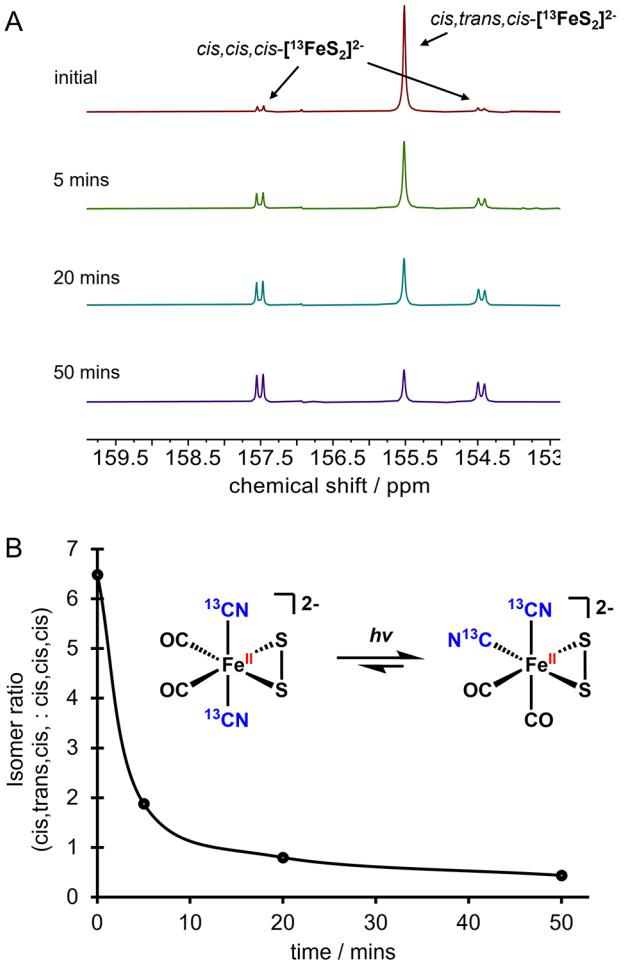

Figure 5. (A) ^{13}C NMR spectra (CN region) for the isomerization of $[K(18\text{-crown-}6)]_2[Fe(S_2)(^{13}CN)_2(CO)_2]$ (CD_3OD solution) at room temperature under white light at the indicated time points. (B) Plot of isomer ratio vs time.

This photoisomerization was accompanied by ∼12% degradation. It is likely that the presence of a *cis,cis,cis* isomer in the initial sample resulted from adventitious photoisomerization.

Reactions of $[Fe(S_2)(CN)_2(CO)_2]^{2-}$ with S_8. FT-IR spectroscopy confirmed that MeCN solutions of $[\mathbf{FeS_2}]^{2-}$ reacted readily with S_8 to give species resembling the aforementioned $[Fe(S_x)(CN)_2(CO)_2]^{2-}$ (eq 1). Additional details were revealed when the reaction of $[^{13}\mathbf{FeS_2}]^{2-}$ with S_8 was followed by ^{13}C NMR spectroscopy (Figure 6). The reaction of $[^{13}\mathbf{FeS_2}]^{2-}$ and S_8 rapidly gave the isomers of

https://doi.org/10.1021/acs.inorgchem.2c00684
Inorg. Chem. 2022, 61, 8241−8249

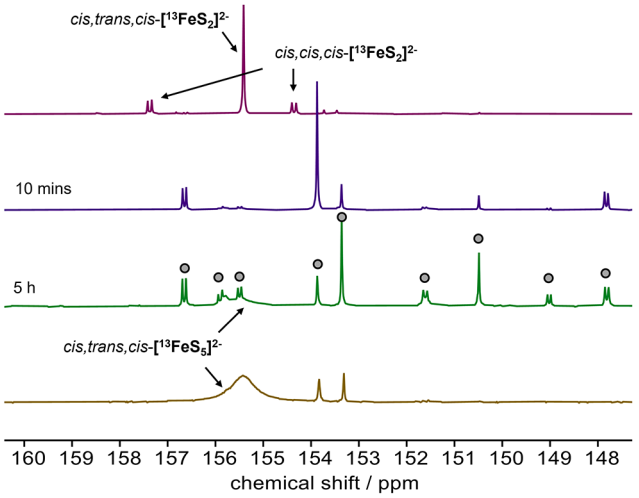

Figure 6. ^{13}C NMR spectra (*C*N region) of the time course of the reaction of $[K(18\text{-crown-}6)]_2[Fe(S_2)(^{13}CN)_2(CO)_3]$ (CD_3OD solution) with S_8 at room temperature under reduced ambient light. Gray circles denote the isomers of $[Fe(S_x)(^{13}CN)_2(CO)_3]^{2-}$ (x = 4–7).

$[Fe(S_x)(CN)_2(CO)_2]^{2-}$ (x = 4–7). *cis,trans,cis*-$[\mathbf{^{13}FeS_5}]^{2-}$ only slowly appears. Previously, the expansion of small MS_x rings by the addition of elemental sulfur had been inferred only from precipitation experiments. For example, addition of elemental sulfur to a DMF solution of $[Mo_2E_2(\mu\text{-}S)_2(S_2)_2]^{2-}$ (E = S or O) followed by crystallization gives $[Mo_2E_2(\mu\text{-}S)_2(S_4)_2]^{2-}$.[23]

$$[Fe(S_2)(CN)_2(CO)_2]^{2-} + (x-2)/8S_8 \rightarrow [Fe(S_x)(CN)_2(CO)_2]^{2-} \quad (x = 4\text{–}7) \qquad (1)$$

$[K(18\text{-crown-}6)]_2[Fe(S\text{-benzyl})_2(CN)_2(CO)_2]$. Complementing the oxidative addition of elemental sulfur, dibenzyl disulfide (Bn_2S_2) adds to $[Fe(CN)_2(CO)_3]^{2-}$. The reaction afforded an 87% yield of $[K(18\text{-crown-}6)]_2[Fe(SBn)_2(CN)_2(CO)_2]$, which was isolated as bright orange crystals (Scheme 3). The method is an improvement over salt-

Scheme 3. Synthesis of $[Fe(SBn)_2(CN)_2(CO)_2]^{2-}$

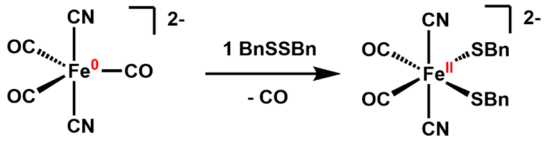

metathesis routes to related complexes.[24,25] Qualitative tests show that *n*-Bu_2S_2, Me_2S_2, and (*p*-tolyl)$_2S_2$ also cleanly add to $[Fe(CN)_2(CO)_3]^{2-}$.

The FT-IR spectrum of a MeCN solution of $[K(18\text{-crown-}6)]_2[Fe(SBn)_2(CN)_2(CO)_2]$ shows ν_{CO} bands at 1996 and 1936 cm^{-1} (Figure 7). The value of ν_{COavg} at 1966 cm^{-1} is lower than that for $[\mathbf{FeS_5}]^{2-}$ (1985 cm^{-1}). The solid-state structure was verified by X-ray crystallography (Figure 7). ∠S(1)–Fe(1)–S(2) is 91.536(16)°. In the ^{1}H NMR spectrum, only the *cis,trans,cis* isomer was detected, with the C*H*$_2$ signal appearing as a singlet (δ 3.64).

Followed by ^{1}H and ^{13}C NMR spectroscopy in a CD_3CN solution of the $[K(18\text{-crown-}6)]^+$ salt, *cis,trans,cis*-$[Fe(SBn)_2(CN)_2(CO)_2]^{2-}$ transforms into an all-*cis* isomer under white LED light. The reaction is quantitative after irradiation for 1.5 h. No isomerization was observed after 3 h

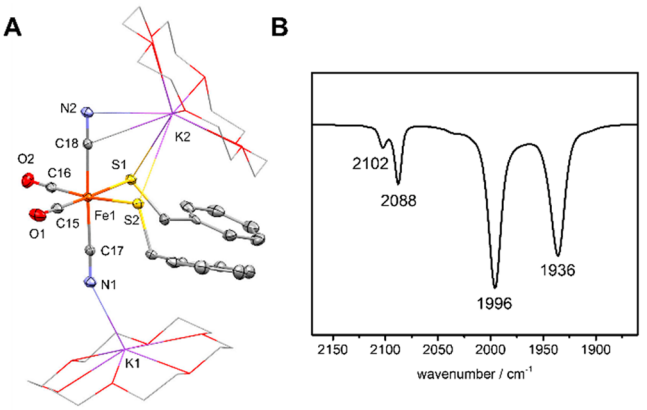

Figure 7. (A) Structure of $[K(18\text{-crown-}6)]_2[Fe(SBn)_2(CN)_2(CO)_2]$. Hydrogen atoms have been omitted for the sake of clarity. Selected distances (angstroms): Fe(1)–C(15), 1.7612(19); Fe(1)–C(16), 1.778(2); Fe(1)–C(17), 1.9401(15); Fe(1)–C(18), 1.9322(15); Fe(1)–S(1), 2.3708(5); Fe(1)–S(2), 2.3661(5). (B) FT-IR spectrum of the same salt in a MeCN solution.

in the absence of light. When the isomerization was repeated under 4 atm of CO, no effect was observed (i.e., the rate was the same). The ^{1}H and ^{13}C NMR spectra of $[K(18\text{-crown-}6)]_2[$*cis,cis,cis*-$Fe(SBn)_2(CN)_2(CO)_2]$ exhibit two sets of signals for each ligand type (Figure S37). ^{13}CN-enriched samples revealed two cyanide doublets ($^2J_{CC}$ = 11.5 Hz) in the ^{13}C NMR spectrum in place of two *C*N singlets for the unlabeled sample, which further confirmed our assignment (Figure 8).

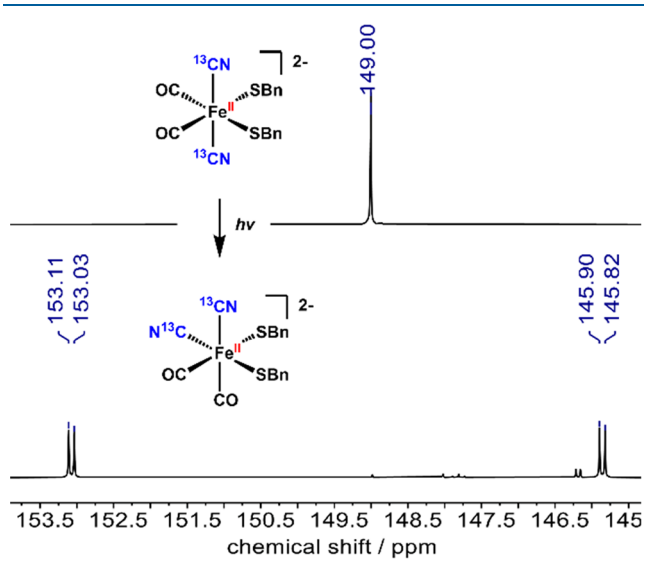

Figure 8. (A) ^{13}C NMR spectra (*C*N region) of $[K(18\text{-crown-}6)]_2[$*cis,trans,cis*-$Fe(SBn)_2(^{13}CN)_2(CO)_2]$ (CD_3CN solution) at room temperature before (top) and after (bottom) exposure to visible light.

$[K(18\text{-crown-}6)]_2[Fe(Se_x)(CN)_2(CO)_2]$. The addition of excess gray Se to a MeCN solution of $[K(18\text{-crown-}6)]_2[Fe(CN)_2(CO)_3]$ gave a deep green solution. The color changed to dark red over the course of hours along with partial dissolution of Se^0. The usual workup afforded red crystals of $[K(18\text{-crown-}6)]_2[Fe(Se_x)(CN)_2(CO)_2]$ (x = 4 or 5). Crystallographic analysis revealed a mixture of octahedral complexes *cis,trans,cis*-$[Fe(Se_4)(CN)_2(CO)_2]^{2-}$ and *cis,trans,*-

https://doi.org/10.1021/acs.inorgchem.2c00684
Inorg. Chem. 2022, 61, 8241–8249

cis-$[Fe(Se_5)(CN)_2(CO)_2]^{2-}$ (Figure 9). The ratio was 72:28. The $FeSe_4$ ring adopted an atypical "envelope" conformation,

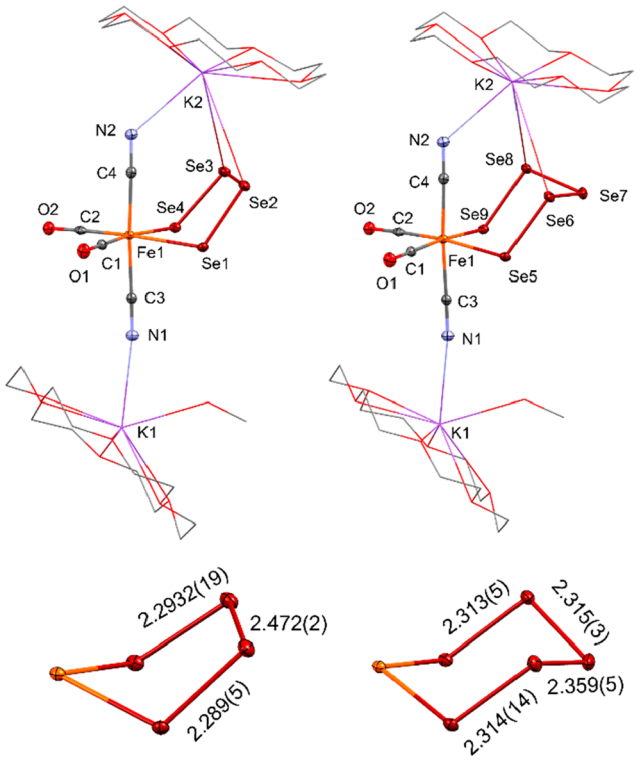

Figure 9. Structure of $[K(18\text{-crown-6})]_2[Fe(Se_x)(CN)_2(CO)_2]\cdot$MeOH ($x$ = 4, left; x = 5, right). Hydrogen atoms have been omitted for the sake of clarity. Selected distances (angstroms): Fe(1)−C(1), 1.780(4); Fe(1)−C(2), 1.767(4); Fe(1)−C(3), 1.944(4); Fe(1)−C(4), 1.928(4); Fe(1)−Se(1), 2.480(5); Fe(1)−Se(4), 2.464(3); Fe(1)−Se(5), 2.458(15); Fe(1)−Se(9), 2.464(6); Se(2)−K(2), 3.670(3); Se(3)−K(2), 3.6811(11); Se(6)−K(2), 3.786(7); Se(8)−K(2), 3.9041(19).

where the four selenium atoms are nearly coplanar (∠Se1−Se2−Se3−Se4 = 1.9°). Most MSe_4 structures adopt "half-chair" conformation. Iron-based examples include $[Fe(Se_4)_2(CO)_2]^{2-}$ (∠Se1−Se2−Se3−Se4 = 56.60°),[26] and $Fe(Se_4)$(phenanthroline)$_2$ has a ∠Se1−Se2−Se3−Se4 of 49.22(3)°.[27] The distinctive structure of this $FeSe_4$ ring is attributed to the $K^+\cdots$Se interaction, even though they are weak ($r_{K\cdots Se}$ > 3.6 Å). The results imply that $FeSe_4$ conformers are similar in energy.

The ^{13}C and ^{77}Se NMR spectra of the $[K(18\text{-crown-6})]_2[Fe(Se_x)(CN)_2(CO)_2]$ samples in a CD_3OD solution were difficult to reproduce until the light and thermal sensitivity were recognized. ^{13}C NMR spectra of freshly dissolved crystalline samples exhibit at least four pairs of CO and CN signals, but exposure of such solutions to ambient light and/or temperature led to the formation of two major species that are assigned to *cis,trans,cis* and *cis,cis,cis* isomers of $[Fe(Se_4)(CN)_2(CO)_2]^{2-}$ [ratio of 5:6 (Figure S14)]. The ^{77}Se NMR spectrum of the same solution revealed six signals in the range of δ 450−750. The integrated intensities (6:6:10:6:6:10) are consistent with the presence of *cis,trans,cis* and *cis,cis,cis* isomers (Figure 10 and Figure S15).

$[Fe(Te_2)(CN)_2(CO)_2]^{2-}$. Addition of excess tellurium powder to a MeCN solution of $[K(18\text{-crown-6})]_2[Fe(CN)_2(CO)_3]$ afforded a dark red solution over the course

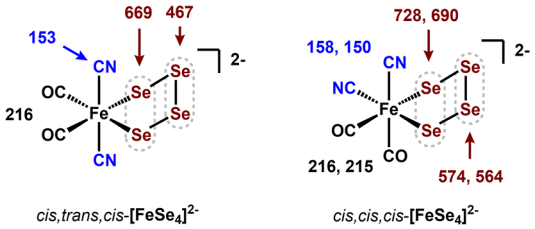

Figure 10. ^{13}C (blue and black) and ^{77}Se NMR (maroon) assignments for $[Fe(Se_4)(CN)_2(CO)_2]^{2-}$ (CD_3OD solution, chemical shifts in parts per million).

of hours at room temperature. An unexceptional workup gave dark orange powders of $[K(18\text{-crown-6})]_2[Fe(Te_2)(CN)_2(CO)_2]$ in 62% yield. Metal tellurido complexes can be labile,[28,29] but solutions of $[K(18\text{-crown-6})]_2[Fe(Te_2)(CN)_2(CO)_2]$ in MeOH appeared to be stable indefinitely at room temperature. The compound is, however, quite sensitive to air.

The solid-state structure of $[K(18\text{-crown-6})]_2[Fe(Te_2)(CN)_2(CO)_2]$ was obtained by X-ray crystallography. Overall, the anionic complex closely resembles $[Fe(S_2)(CN)_2(CO)_2]^{2-}$, where the pertelluride ligand is encapsulated by two K(18-crown-6)$^+$ (Figure 12A). The Te−Te bond length of 2.6965(2) Å is similar to that of the only other monoiron pertellurides, $Fe(Te_2)(R_2PCH_2CH_2PR_2)_2$ (R = Me or Et).[30]

While only the C_{2v} symmetric *cis,trans,cis* isomer of $[Fe(Te_2)(CN)_2(CO)_2]^{2-}$ was found in the solid state, the ^{13}C NMR spectrum of $[K(18\text{-crown-6})]_2[Fe(Te_2)(CN)_2(CO)_2]$ shows three *CO* and three *CN* resonances, consistent with a mixture of all-*cis* and *cis,trans,cis* isomers (Figure 11). The ^{125}Te NMR spectrum recorded for the same

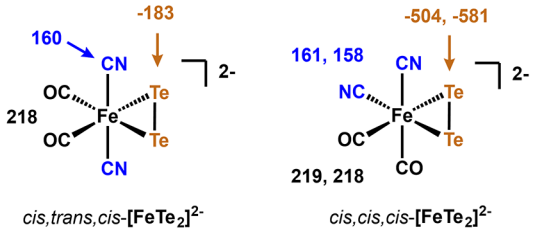

Figure 11. ^{13}C (blue and black) and ^{125}Te (brown) NMR assignments for $[Fe(Te_2)(CN)_2(CO)_2]^{2-}$ (CD_3OD solution, chemical shifts in parts per million).

sample revealed three signals, as well (δ −183, −504, and −571). The two upfield resonances are similarly intense, consistent with an all-*cis* isomer where two tellurium atoms are chemically inequivalent. The ratio of two isomers changes over time under ambient light, which eventually reaches ∼4:1 (*cis,cis,cis*:*cis,trans,cis*).

To evaluate the effect of cations, $(Et_4N)_2[Fe(Te_2)(CN)_2(CO)_2]$ was also prepared from $(Et_4N)_2[Fe(CN)_2(CO)_3]$ and Te powder. In contrast to the K(18-crown-6)$^+$ salt, $(Et_4N)_2[Fe(Te_2)(CN)_2(CO)_2]$ crystallizes as the chiral all-*cis* isomer (Figure 12B). The interactions between the dianionic complex with $[K(18\text{-crown-6})]^+$ influence the isomer ratio. Because these interactions appear to be weak, the two isomers of $[Fe(Te_2)(CN)_2(CO)_2]^{2-}$ differ only slightly in energy. In a methanol solution, the NMR and FT-IR

https://doi.org/10.1021/acs.inorgchem.2c00684
Inorg. Chem. 2022, 61, 8241−8249

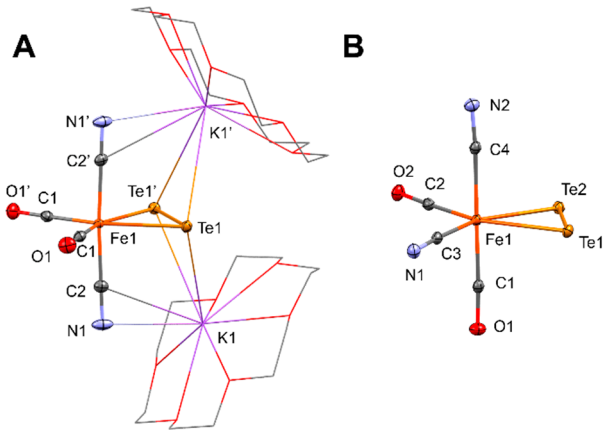

Figure 12. (A) Structure of $[K(18\text{-crown-6})]_2[cis,trans,cis\text{-}Fe(Te_2)(CN)_2(CO)_2]$. Selected distances (angstroms): Te(1)−Fe(1), 2.6354(3); Te(1)-Te(1′), 2.6965(2); Fe(1)−C(1), 1.7769(19); Fe(1)−C(2), 1.9202(19). (B) Structure of the anion in $(Et_4N)_2[cis,cis,cis\text{-}Fe(Te_2)(CN)_2(CO)_2]$. Selected distances (angstroms): Te(1)−Fe(1), 2.6423(3); Te(1)−Te(2), 2.70525(17); Te(2)−Fe(1), 2.6379(3); Fe(1)−C(1), 1.7899(19); Fe(1)−C(2), 1.7620(19); Fe(1)−C(3), 1.9222(19); Fe(1)−C(4), 1.9507(18).

spectroscopic properties of the Et_4N^+ and $[K(18\text{-crown-6})]^+$ salts are very similar.

Treatment of a MeCN solution of $(Et_4N)_2[Fe(Te_2)(CN)_2(CO)_2]$ with elemental sulfur resulted in the rapid formation of a dark-gray precipitate, which we attribute to elemental Te. According to FT-IR analysis, the reaction quantitatively produced $[Fe(S_x)(CN)_2(CO)_2]^{2-}$, as summarized in simplified eq 2.

$$[Fe(Te_2)(CN)_2(CO)_2]^{2-} + x/8S_8 \rightarrow [Fe(S_x)(CN)_2(CO)_2]^{2-} + 2Te \quad (x = 4\text{–}7) \qquad (2)$$

Closing Remarks. This report introduces a new family of octahedral ferrous chalcogenide complexes. Although the paper emphasizes the inorganic polychalcogenides, the addition of dibenzyl disulfide suggests that the iron(0) dicyanide will add a range of substrates containing chalcogen−chalcogen bonds.

The new complexes feature spectator CN^- and CO ligands that report on the stereochemistry and electronic character, respectively, of the complexes. It is obvious that polychalcogen complexes could exist as geometric isomers, but this phenomenon had not been observed previously. Few polychalcogenide complexes are heteroleptic (i.e., mixed ligand) and octahedral, which are suitable for isomerism. Three clear examples are demonstrated in this work, as observed by ^{13}C and $^{77}Se/^{125}Te$ NMR spectroscopy: $[Fe(S_2)(CN)_2(CO)_2]^{2-}$, $[Fe(Se_4)(CN)_2(CO)_2]^{2-}$, and $[Fe(Te_2)(CN)_2(CO)_2]^{2-}$ exist in solution as mixtures of the *cis,cis,cis* and *cis,trans,cis* isomers. In terms of their electronic properties, CN^- and the polychalcogenide are apparently similar electronically;[31,32] hence, the CO ligands are "ambivalent" with regard to their stereochemistry (i.e., being *trans* to chalcogenide vs CN^- is similar energetically).

The $[K(18\text{-crown-6})]^+$ salts of $[Fe(S_5)(CN)_2(CO)_2]^{2-}$, $[Fe(S_2)(CN)_2(CO)_2]^{2-}$, and $[Fe(SBn)_2(CN)_2(CO)_2]^{2-}$ have the same stereochemistry at Fe, allowing comparison of their IR spectra in the ν_{CO} region. The following trend is observed for ν_{COavg}: S_2^{2-} (1960 cm^{-1}) < 2SBn$^-$ (1966 cm^{-1}) < S_5^{2-} (1985 cm^{-1}). The donor properties of S_x^{2-} are strongly affected by the value of x: persulfide (S_2^{2-}) is a stronger donor than higher polysulfides, being more comparable to alkylthiolate. The fact that the higher polysulfides are similar electronically is consistent with the easy equilibration of the FeS_x species for x = 4−7, as observed in this study and other studies.[33,34] We also observe that ν_{COavg} is significantly lower (12 cm^{-1}) for the Te_2^{2-} complex than for the analogous S_2^{2-} derivative, indicating that the heavier dichalcogenide is a superior electron donor.

We describe unique examples of photoisomerization of metal chalcogenide and thiolato complexes. The photoreactivity is associated with the metal center, not the chalcogen−chalcogen bonds as indicated by the similar behavior for the benzylthiolate complex.

EXPERIMENTAL SECTION

Materials. Synthetic manipulations were carried out using standard Schlenk techniques or in an MBraun drybox under an atmosphere of purified nitrogen. Operations were conducted at room temperature unless otherwise indicated. Solvents for air- and moisture-sensitive manipulations were dried and deoxygenated using an MBraun Solvent Purification System and stored over 4 Å molecular sieves. For the synthetic procedures, solvent volumes are approximate. All operations were conducted at room temperature unless indicated otherwise. The salt $[K(18\text{-crown-6})]_2[Fe(CN)_2(CO)_3]$ was prepared according to ref 14.

Physical Measurements. ^1H and $^{13}C\{^1H\}$ NMR spectra were recorded on Varian UNITY INOVA 500 MHz, Varian Inova 600 MHz, and Bruker Ascend 600 MHz spectrometers. All chemical shifts are reported using the δ scale (parts per million) relative to $SiMe_4$ using ^1H (residual) chemical shifts of the solvent as a secondary standard. Coupling constants (J) are reported in hertz. Elemental analysis was performed by the School of Chemical Sciences Microanalysis Laboratory utilizing a model CE 440 CHN analyzer. Solution IR spectra were recorded on a PerkinElmer Spectrum 100 FT-IR spectrometer and are reported in inverse centimeters. Gas chromatography (GC) data were collected using an HP 6890 Series GC System.

Preparation of $[K(18\text{-crown-6})]_2[Fe(S_5)(CN)_2(CO)_2]$. In a drybox, $[K(18\text{-crown-6})]_2[Fe(CN)_2(CO)_3]$ (205 mg, 0.257 mmol, 1.0 equiv) and S_8 (64 mg, 0.251 mmol, 0.98 equiv) were loaded in a 20 mL vial followed by 8 mL of MeCN. The reaction mixture was stirred for 4 h. The excess of sulfur was filtered off. The solvent was removed, and the residue was redissolved in 3 mL of MeOH. Approximately 10 mL of Et_2O was layered atop the MeOH solution. After standing for 15 h, the solution was decanted, and the orange crystals of $[K(18\text{-crown-6})]_2[Fe(S_5)(CN)_2(CO)_2]$ were rinsed with THF (2 × 1 mL) and Et_2O (1 × 2 mL). After the solid product had been dried under vacuum, the yield was 133 mg (56%). IR (MeCN, N_2): 2108 (m, CN), 2094 (m, CN), 2013 (s, CO), 1956 (vs, CO). IR (MeOH, air): 2110 (m, CN), 2093 (m, CN), 2027 (s, CO), 1978 (vs, CO). IR (H_2O, air): 2108 (m, CN), 2088 (m, CN), 2043 (s, CO), 1998 (vs, CO). ^1H NMR (600 MHz, CD_3OD): δ 3.64 (s, 48H, OCH_2CH_2O). ^{13}C NMR (151 MHz, CD_3OD): δ 214, 213, 212, 155, 154, 153, 71.3. Anal. Calcd for $C_{28}H_{48}FeK_2N_2O_{14}S_5\cdot CH_4O$: C, 36.17; H, 5.44; N, 2.91. Found: C, 36.01; H, 5.52; N, 2.96. Single crystals suitable for crystallographic analysis were grown by layering a MeCN solution of $[K(18\text{-crown-6})]_2[Fe(S_5)(CN)_2(CO)_2]$ with Et_2O.

Preparation of $[K(18\text{-crown-6})]_2[Fe(S_5)(^{13}CN)_2(CO)_2]$. In a drybox, $[K(18\text{-crown-6})]_2[Fe(^{13}CN)_2(CO)_3]$ (200 mg, 0.250 mmol, 1.0 equiv) and S_8 (64 mg, 0.250 mmol, 1.0 equiv) were loaded in a 20 mL vial followed by 8 mL of MeCN. The reaction mixture was stirred for 4 h. The excess of sulfur was filtered off. The solvent was removed, and the residue was redissolved in 3 mL of MeOH. Approximately 10 mL of Et_2O was layered atop the MeOH solution. After standing for 15 h, the solution was decanted, and the orange microcrystals of $[K(18\text{-crown-6})]_2[Fe(S_5)(^{13}CN)_2(CO)_2]$ were rinsed with THF (2 × 1 mL) and Et_2O (1 × 2 mL). After the product had been dried under

https://doi.org/10.1021/acs.inorgchem.2c00684
Inorg. Chem. 2022, 61, 8241−8249

vacuum, the yield was 150 mg (64%). IR (MeCN): 2064 (m, CN), 2050 (m, CN), 2011 (s, CO), 1956 (vs, CO). ^{1}H NMR (600 MHz, CD_3OD): δ 3.64 (s, 48H, OCH_2CH_2O). ^{13}C NMR (151 MHz, CD_3OD): δ 212.65 (t, J = 9.9), 155.42, 153.83, 153.31, 71.35 (CO resonances for minor species are not detected). Anal. Calcd for $C_{26}{}^{13}C_2H_{48}FeK_2N_2O_{14}S_5{\cdot}CH_4O$: C, 36.30; H, 5.43; N, 2.90. Found: C, 36.18; H, 5.50; N, 3.10.

Preparation of [K(18-crown-6)]$_2$[Fe(S$_2$)(CN)$_2$(CO)$_2$]. In a drybox, [K(18-crown-6)]$_2$[Fe(CN)$_2$(CO)$_3$] (261 mg, 0.327 mmol, 1.0 equiv) and S_8 (21 mg, 0.082 mmol, 0.25 equiv) were loaded in a 20 mL vial followed by 5 mL of MeCN. The reaction mixture was stirred for 6 h. The reaction mixture was filtered, and ∼10 mL of Et_2O was layered atop the filtrate. After standing for 2 days, the solution was decanted, and the remaining [K(18-crown-6)]$_2$[Fe(S$_2$)(CN)$_2$(CO)$_2$] solids were rinsed with Et_2O (3 × 2 mL). After the sample had been dried under vacuum, the dark orange crystals of [K(18-crown-6)]$_2$[Fe(S$_2$)(CN)$_2$(CO)$_2$] were collected. Yield: 180 mg (66%). IR (MeCN): 2101 (m, CN), 2087 (m, CN), 1994 (s, CO), 1925 (vs, CO). ^{1}H NMR (600 MHz, CD_3OD): δ 3.64 (s, OCH_2CH_2O). ^{13}C NMR (151 MHz, CD_3OD): δ 217, 217, 211, 157, 155, 154, 71.4. Anal. Calcd for $C_{28}H_{48}FeK_2N_2O_{14}S_2{\cdot}1.5C_2H_3N$: C, 41.54; H, 5.90; N, 5.47. Found: C, 42.20; H, 6.05; N, 5.36. Single crystals suitable for crystallographic analysis were grown by layering a MeCN solution of [K(18-crown-6)]$_2$[Fe(S$_2$)(CN)$_2$(CO)$_2$] with Et_2O.

Preparation of [K(18-crown-6)]$_2$[Fe(S$_2$)(^{13}CN)$_2$(CO)$_2$]. In a drybox, [K(18-crown-6)]$_2$[Fe(^{13}CN)$_2$(CO)$_3$] (100 mg, 0.125 mmol, 1.0 equiv) and S_8 (8 mg, 0.031 mmol, 0.25 equiv) were loaded in a 20 mL vial followed by 5 mL of MeCN. The reaction mixture was stirred for 6 h. The reaction mixture was filtered, and ∼10 mL of Et_2O was layered atop the filtrate. After standing for 1 day, the solution was decanted, and the orange crystals of [K(18-crown-6)]$_2$[Fe(S$_2$)(^{13}CN)$_2$(CO)$_2$] solids were rinsed with Et_2O (3 × 2 mL). After the crystals had been dried under vacuum, the yield was 50 mg (48%). IR (MeCN): 2058 (m, CN), 2042 (m, CN), 1992 (s, CO), 1924 (vs, CO). ^{1}H NMR (600 MHz, CD_3OD): δ 3.64 (s, OCH_2CH_2O). ^{13}C NMR (151 MHz, CD_3OD): δ 216.57 (t, J = 11.4), 157 (d, J = 13.2), 155, 154 (d, J = 13.3). CO resonances for minor species were not detected. Anal. Calcd for $C_{26}{}^{13}C_2H_{48}FeK_2N_2O_{14}S_2{\cdot}1.5C_2H_3N$: C, 41.66; H, 5.89; N, 5.46. Found: C, 41.98; H, 6.05; N, 5.06.

Preparation of [K(18-crown-6)]$_2$[Fe(SBn)$_2$(CN)$_2$(CO)$_2$]. In a drybox, [K(18-crown-6)]$_2$[Fe(CN)$_2$(CO)$_3$] (1.5 g, 1.88 mmol, 1.0 equiv) and Bn_2S_2 (463 mg, 1.88 mmol, 1.0 equiv) were loaded in a 20 mL vial followed by 15 mL of MeCN. The reaction mixture was stirred for 3 h. The solution was concentrated to a volume of ∼5 mL, and Et_2O (∼10 mL) was added to precipitate the product. After standing for 16 h, the solution was decanted, and the yellow-orange microcrystals of [K(18-crown-6)]$_2$[Fe(SBn)$_2$(CN)$_2$(CO)$_2$] were rinsed with THF/Et_2O (3 × 2 mL). After the solid had been dried under vacuum, the yield was 1.66 g (87%). IR (MeCN): 2102 (m, CN), 2088 (m, CN), 1996 (s, CO), 1936 (vs, CO). ^{1}H NMR (600 MHz, CD_3CN): δ 7.41 (d, J = 7.4, 4H), 7.18 (t, J = 7.6, 4H), 7.05 (t, J = 7.3, 2H), 3.64 (s, 4H), 3.55 (s, 48H). ^{13}C NMR (151 MHz, CD_3CN): δ 217, 149, 149, 130, 128, 125, 70.8, 36.9. Anal. Calcd for $C_{42}H_{62}FeK_2N_2O_{14}S_2$: C, 49.60; H, 6.14; N, 2.75. Found: C, 49.46; H, 6.14; N, 3.17. Single crystals suitable for crystallographic analysis were grown by layering a MeCN solution of [K(18-crown-6)]$_2$[Fe(SBn)$_2$(CN)$_2$(CO)$_2$] with Et_2O at −35 °C.

Preparation of [K(18-crown-6)]$_2$[Fe(SBn)$_2$(^{13}CN)$_2$(CO)$_2$]. In a drybox, [K(18-crown-6)]$_2$[Fe(^{13}CN)$_2$(CO)$_3$] (200 mg, 0.25 mmol, 1.0 equiv) and BnSSBn (62 mg, 0.25 mmol, 1.0 equiv) were loaded in a 20 mL vial followed by 3 mL of MeCN. The reaction mixture was stirred for 3 h. The solution was concentrated to ∼1 mL, and Et_2O (∼12 mL) was added to precipitate the product. After standing for 16 h, the solution was decanted, and the orange microcrystals of [K(18-crown-6)]$_2$[Fe(SBn)$_2$(^{13}CN)$_2$(CO)$_2$] were rinsed with Et_2O (3 × 2 mL). After the product had been dried under vacuum, the yield was 225 mg (88%). IR (MeCN): 2058 (m, CN), 2043 (m, CN), 1994 (s, CO), 1936 (vs, CO). ^{1}H NMR (600 MHz, CD_3CN): δ 7.40 (d, J = 7.2, 4H), 7.18 (t, J = 7.6, 4H), 7.05 (t, J = 7.3, 2H), 3.63 (s, 4H), 3.55 (s, 48H). ^{13}C NMR (151 MHz, CD_3CN): δ 217 (t, J = 9.8), 149.0, 148.8, 130, 128, 125, 70.9, 36.9 (t, J = 2.0). Anal. Calcd for $C_{40}{}^{13}C_2H_{62}FeK_2N_2O_{14}S_2$: C, 49.70; H, 6.13; N, 2.75. Found: C, 49.32; H, 6.06; N, 2.97.

Preparation of [K(18-crown-6)]$_2$[Fe(Se$_x$)(CN)$_2$(CO)$_2$] (x = 4 or 5). In a drybox, [K(18-crown-6)]$_2$[Fe(CN)$_2$(CO)$_3$] (265 mg, 0.332 mmol, 1.0 equiv) and Se (210 mg, 2.65 mmol, 8.0 equiv) were loaded in a 20 mL vial followed by 10 mL of MeCN. The reaction mixture was stirred for 16 h. The excess of Se was filtered off. The solvent was removed, and the residue was redissolved in 3 mL of MeOH. Approximately 10 mL of Et_2O was layered atop the MeOH solution. After standing for 16 h, the solution was decanted, and the red-colored microcrystals of [K$_2$(18-crown-6)$_2$(MeCN)][Fe(Se$_x$)(CN)$_2$(CO)$_2$] were rinsed with THF (2 × 1 mL) and Et_2O (1 × 2 mL). After the product had been dried under vacuum, the yield was 233 mg (65%). IR (MeCN, fresh sample): 2105 (m, CN), 2092 (m, CN), 2004 (s, CO), 1949 (s, CO). IR (MeCN, irradiated sample): 2105 (m, CN), 2092 (m, CN), 2004 (s, CO), 1949 (s, CO). ^{1}H NMR (600 MHz, CD_3OD, irradiated): δ 3.64 (s, OCH_2CH_2O). ^{13}C NMR (151 MHz, CD_3CN, irradiated): δ 216, 216, 214.56, 158, 152, 150, 71.4. ^{77}Se NMR (115 MHz, CD_3OD, irradiated): δ 728, 690, 669, 574, 564, 467. Anal. Calcd for $C_{28}H_{48}FeK_2N_2O_{14}Se_4$: C, 30.95; H, 4.45; N, 2.58. Found: C, 30.77; H, 4.47; N, 2.65. Single crystals suitable for crystallographic analysis were grown by layering a MeOH solution of [K(18-crown-6)]$_2$[Fe(Se$_x$)(CN)$_2$(CO)$_2$] with Et_2O.

Preparation of [K(18-crown-6)]$_2$[Fe(Te$_2$)(CN)$_2$(CO)$_2$]. In a drybox, [K(18-crown-6)]$_2$[Fe(CN)$_2$(CO)$_3$] (200 mg, 0.250 mmol, 1.0 equiv) and Te (160 mg, 1.25 mmol, 5.0 equiv) were loaded in a 20 mL vial followed by 4 mL of MeOH. The reaction mixture was stirred for 16 h. The excess of Te was filtered off. The solvent was removed, and the residue was redissolved in 3 mL of MeOH. Approximately 10 mL of Et_2O was layered atop the MeOH solution. After standing for 1 day, the solution was decanted, and the red-orange solid [K$_2$(18-crown-6)$_2$(MeCN)][Fe(Te$_2$)(CN)$_2$(CO)$_2$] was rinsed with 1:1 MeCN/Et_2O (2 × 2 mL) and Et_2O (1 × 2 mL). After the solids had been dried under vacuum, the yield was 160 mg (62%). IR (MeCN): 2097 (m, CN), 2088 (m, CN), 1978 (s, CO), 1919 (vs, CO). ^{1}H NMR (600 MHz, CD_3OD): δ 3.64 (s, OCH_2CH_2O). ^{13}C NMR (126 MHz, CD_3OD): δ 218, 218, 217, 161, 160, 158, 71.4. ^{125}Te NMR (158 MHz, CD_3OD): δ −183, −504, −571. Anal. Calcd for $C_{28}H_{48}FeK_2N_2O_{14}Te_2{\cdot}C_2H_3N$: C, 33.77; H, 4.82; N, 3.94. Found: C, 33.78; H, 4.74; N, 4.17. Single crystals suitable for crystallographic analysis were grown by layering a MeOH solution of [K(18-crown-6)]$_2$[Fe(Te$_2$)(CN)$_2$(CO)$_2$] with Et_2O.

Preparation of (Et$_4$N)$_2$[Fe(Te$_2$)(CN)$_2$(CO)$_2$]. In a drybox, (Et$_4$N)$_2$[Fe(CN)$_2$(CO)$_3$] (160 mg, 0.354 mmol, 1.0 equiv) and Te (239 mg, 1.87 mmol, 5.3 equiv) were loaded in a 20 mL vial followed by 5 mL of MeCN. The reaction mixture was stirred for 24 h. The excess of Te was filtered off, and the filtrate was concentrated. Approximately 8 mL of Et_2O was layered on the MeCN solution. After standing for 1 day, the Et_2O/MeCN solution deposited crystals of (Et$_4$N)$_2$[Fe(Te$_2$)(CN)$_2$(CO)$_2$]. Solvents were decanted, and the red-purple microcrystals were rinsed with THF (2 × 2 mL) and Et_2O (1 × 2 mL). After the solids had been dried under vacuum, the yield was 214 mg (89%). IR (MeCN): 2097 (m, CN), 2088 (m, CN), 1978 (s, CO), 1920 (vs, CO). ^{1}H NMR (600 MHz, CD_3CN): δ 3.21 (q, J = 7.2, 16H, NCH_2), 1.22 (t, J = 6.4, 24H, CH_3). ^{13}C NMR (151 MHz, CD_3CN): δ 221, 220, 218.89, 151, 148, 145, 53.1, 7.84. ^{125}Te NMR (158 MHz, CD_3CN): δ −105, −464, −523. ^{125}Te NMR (158 MHz, CD_3OD): δ −172, −505, −552. Anal. Calcd for $C_{20}H_{40}FeN_4O_2Te_2{\cdot}C_2H_3N$: C, 36.67; H, 6.01; N, 9.72. Found: C, 36.41; H, 5.99; N, 9.47. Single crystals suitable for crystallographic analysis were grown by layering a MeCN solution of (Et$_4$N)$_2$[Fe(Te$_2$)(CN)$_2$(CO)$_2$] with Et_2O.

■ ASSOCIATED CONTENT

Supporting Information

The Supporting Information is available free of charge at https://pubs.acs.org/doi/10.1021/acs.inorgchem.2c00684.

https://doi.org/10.1021/acs.inorgchem.2c00684
Inorg. Chem. 2022, 61, 8241−8249

NMR, ESI-MS, and additional IR spectra (PDF)

Accession Codes

CCDC 2154881−2154886 contain the supplementary crystallographic data for this paper. These data can be obtained free of charge via www.ccdc.cam.ac.uk/data_request/cif, or by emailing data_request@ccdc.cam.ac.uk, or by contacting The Cambridge Crystallographic Data Centre, 12 Union Road, Cambridge CB2 1EZ, UK; fax: +44 1223 336033.

AUTHOR INFORMATION

Corresponding Author

Thomas B. Rauchfuss − *School of Chemical Sciences, University of Illinois, Urbana, Illinois 61801, United States;* orcid.org/0000-0003-2547-5128; Email: rauchfuz@illinois.edu

Authors

Yu Zhang − *School of Chemical Sciences, University of Illinois, Urbana, Illinois 61801, United States;* orcid.org/0000-0001-8948-1434

Toby Woods − *School of Chemical Sciences, University of Illinois, Urbana, Illinois 61801, United States;* orcid.org/0000-0002-1737-811X

Complete contact information is available at: https://pubs.acs.org/10.1021/acs.inorgchem.2c00684

Notes

The authors declare no competing financial interest.

ACKNOWLEDGMENTS

This work was supported by the National Institutes of Health (GM-61153).

REFERENCES

(1) Rickard, D.; Luther, G. W. Chemistry of Iron Sulfides. *Chem. Rev.* **2007**, *107*, 514−562.

(2) Coucouvanis, D.; Swenson, D.; Stremple, P.; Baenziger, N. C. Reaction of $[Fe(SC_6H_5)_4]^{2-}$ with Organic Trisulfides and Implications Concerning the Biosynthesis of Ferredoxins. Synthesis and Structure of the $[(C_6H_5)_4P]_2Fe_2S_{12}$ Complex. *J. Am. Chem. Soc.* **1979**, *101*, 3392−3394.

(3) Coucouvanis, D.; Baenziger, N. C.; Simhon, E. D.; Stremple, P.; Swenson, D.; Kostikas, A.; Simopoulos, A.; Petrouleas, V.; Papaefthymiou, V. Heterodinuclear Di-μ-Sulfido Bridged Dimers Containing Iron and Molybdenum or Tungsten. Structures of $(Ph_4P)_2(FeMS_9)$ Complexes (M = Molybdenum, Tungsten). *J. Am. Chem. Soc.* **1980**, *102*, 1730−1732.

(4) Tsai, M.-L.; Chen, C.-C.; Hsu, I.-J.; Ke, S.-C.; Hsieh, C.-H.; Chiang, K.-A.; Lee, G.-H.; Wang, Y.; Chen, J.-M.; Lee, J.-F.; Liaw, W.-F. Photochemistry of the Dinitrosyl Iron Complex $[S_5Fe(NO)_2]^-$ Leading to Reversible Formation of $[S_5Fe(\mu\text{-}S)_2FeS_5]^{2-}$: Spectroscopic Characterization of Species Relevant to the Nitric Oxide Modification and Repair of [2Fe-2S] Ferredoxins. *Inorg. Chem.* **2004**, *43*, 5159−5167.

(5) van den Berg, W.; Boot, L.; Joosen, H.; van der Linden, J. G. M.; Bosman, W. P.; Smits, J. M. M.; de Gelder, R.; Beurskens, P. T.; Heck, J.; Gal, A. W. Iron-Sulfur Clusters with $SiMe_2$-Bridged Cyclopentadienyl Ligands: $[Me_2Si(\eta^5\text{-}C_5H_4)_2]_2Fe_5S_{12}$, $[Me_2Si(\eta^5\text{-}C_5H_4)_2]_2Fe_4S_6$, and $[Me_2Si(\eta^5\text{-}C_5H_4)_2]_2Fe_4S_6(CO)$. *Inorg. Chem.* **1997**, *36*, 1821−1828.

(6) Zhang, Y.; Tao, L.; Woods, T. J.; Britt, R. D.; Rauchfuss, T. B. Organometallic $Fe_2(\mu\text{-}SH)_2(CO)_4(CN)_2$ Cluster Allows the Biosynthesis of the [FeFe]-Hydrogenase with Only the HydF Maturase. *J. Am. Chem. Soc.* **2022**, *144*, 1534−1538.

(7) Rohac, R.; Martin, L.; Liu, L.; Basu, D.; Tao, L.; Britt, R. D.; Rauchfuss, T. B.; Nicolet, Y. Crystal Structure of the [FeFe]-Hydrogenase Maturase HydE Bound to Complex-B. *J. Am. Chem. Soc.* **2021**, *143*, 8499−8508.

(8) Tao, L.; Pattenaude, S. A.; Joshi, S.; Begley, T. P.; Rauchfuss, T. B.; Britt, R. D. Radical SAM Enzyme HydE Generates Adenosylated Fe(I) Intermediates En Route to the [FeFe]-Hydrogenase Catalytic H-Cluster. *J. Am. Chem. Soc.* **2020**, *142*, 10841−10848.

(9) Rao, G.; Pattenaude, S. A.; Alwan, K.; Blackburn, N. J.; Britt, R. D.; Rauchfuss, T. B. The Binuclear Cluster of [FeFe] Hydrogenase is Formed with Sulfur Donated by Cysteine of an $[Fe(Cys)(CO)_2(CN)]$ Organometallic Precursor. *Proc. Natl. Acad. Sci. U.S.A.* **2019**, *116*, 20850.

(10) Artero, V.; Berggren, G.; Atta, M.; Caserta, G.; Roy, S.; Pecqueur, L.; Fontecave, M. From Enzyme Maturation to Synthetic Chemistry: The Case of Hydrogenases. *Acc. Chem. Res.* **2015**, *48*, 2380−2387.

(11) Peters, J. W.; Schut, G. J.; Boyd, E. S.; Mulder, D. W.; Shepard, E. M.; Broderick, J. B.; King, P. W.; Adams, M. W. W. [FeFe]- and [NiFe]-Hydrogenase Diversity, Mechanism, and Maturation. *Biochim. Biophys. Acta - Mol. Cell Res.* **2015**, *1853*, 1350−1369.

(12) Arrigoni, F.; Zampella, G.; Zhang, F.; Kagalwala, H. N.; Li, Q.-L.; Woods, T. J.; Rauchfuss, T. B. Computational and Experimental Investigations of the $Fe_2(\mu\text{-}S_2)/Fe_2(\mu\text{-}S)_2$ Equilibrium. *Inorg. Chem.* **2021**, *60*, 3917−3926.

(13) Kayal, A.; Rauchfuss, T. B. Protonation Studies of the New Iron Carbonyl Cyanide *trans*-$[Fe(CO)_3(CN)_2]^{2-}$: Implications with Respect to Hydrogenases. *Inorg. Chem.* **2003**, *42*, 5046−5048.

(14) Whaley, C. M.; Rauchfuss, T. B.; Wilson, S. R. Coordination Chemistry of $[HFe(CN)_2(CO)_3]^-$ and Its Derivatives: Toward a Model for the Iron Subsite of the [NiFe]-Hydrogenases. *Inorg. Chem.* **2009**, *48*, 4462−4469.

(15) Steudel, R. Homocyclic Sulfur Molecules. *Topics Curr. Chem.* **1982**, *102*, 149.

(16) Wächtershäuser, G. *From Chemical Invariance to Genetic Variability in Bioinspired Catalysis*; Weigand, W., Schollhammer, P., Eds.; Wiley-VCH: Weinheim, Germany, 2014; pp 1−20.

(17) Steudel, R.; Chivers, T. The Role of Polysulfide Dianions and Radical Anions in the Chemical, Physical and Biological Sciences, Including Sulfur-Based Batteries. *Chem. Soc. Rev.* **2019**, *48*, 3279−3319.

(18) Chen, T.-N.; Lo, F.-C.; Tsai, M.-L.; Shih, K.-N.; Chiang, M.-H.; Lee, G.-H.; Liaw, W.-F. Dinitrosyl iron complexes $[E_5Fe(NO)_2]^-$ (E = S, Se): A Precursor of Roussin's black salt $[Fe_4E_3(NO)_7]$. *Inorg. Chim. Acta* **2006**, *359*, 2525−2533.

(19) Fehlhammer, W. P.; Fritz, M. Emergence of a CNH and Cyano Complex Based Organometallic Chemistry. *Chem. Rev.* **1993**, *93*, 1243−1280.

(20) Mascharak, P. K. Convenient Synthesis of Tris-(tetraethylammonium) Hexacyanoferrate(III) and Its Use as an Oxidant with Tunable Redox Potential. *Inorg. Chem.* **1986**, *25*, 245−247.

(21) Contakes, S. M.; Hsu, S. C. N.; Rauchfuss, T. B.; Wilson, S. R. Preparative and Structural Studies on the Carbonyl Cyanides of Iron, Manganese, and Ruthenium: Fundamentals Relevant to the Hydrogenases. *Inorg. Chem.* **2002**, *41*, 1670−1678.

(22) Abel, E. W.; Bhargava, S. K.; Orrell, K. G. The Stereodynamics of Metal Complexes of Sulfur-, Selenium-, and Tellurium-Containing Ligands. *Prog. Inorg. Chem.* **2007**, 1−118.

(23) Coucouvanis, D. Syntheses, Structures, and Reactions of Binary and Tertiary Thiomolybdate Complexes Containing the (O)Mo(S_x) AND (S)Mo(S_x) Functional Groups (x = 1, 2, 4). *Adv. Inorg. Chem.* **1998**, *45*, 1−73.

(24) Rauchfuss, T. B.; Contakes, S. M.; Hsu, S. C. N.; Reynolds, M. A.; Wilson, S. R. The Influence of Cyanide on the Carbonylation of Iron(II): Synthesis of Fe-SR-CN-CO Centers Related to the Hydrogenase Active Sites. *J. Am. Chem. Soc.* **2001**, *123*, 6933−6934.

(25) Jiang, J.; Maruani, M.; Solaimanzadeh, J.; Lo, W.; Koch, S. A.; Millar, M. Synthesis and Structure of Analogues for the Ni-Fe Site in Hydrogenase Enzymes. *Inorg. Chem.* **2009**, *48*, 6359.
(26) Rauchfuss, T. B.; Dev, S.; Wilson, S. R. *N*-Methylimidazole-Promoted Reactions of Iron and Nickel Carbonyls with Chalcogens: Interconversions of Iron Polysulfide Complexes and the Structure of $[FeSe_8(CO)_2]^{2-}$. *Inorg. Chem.* **1992**, *31*, 153−154.
(27) Liu, G.-N.; Zhu, W.-J.; Zhang, M.-J.; Xu, B.; Liu, Q.-S.; Zhang, Z.-W.; Li, C. Syntheses, Crystal and Band Structures, and Optical Properties of a Selenidoantimonate and an Iron Polyselenide. *J. Solid State Chem.* **2014**, *218*, 109−115.
(28) Kolis, J. W. Coordination Chemistry of Polychalcogen Anions and Transition Metal Carbonyls. *Coord. Chem. Rev.* **1990**, *105*, 195−219.
(29) Kanatzidis, M. G.; Huang, S. P. Coordination Chemistry of Heavy Polychalcogenide Ligands. *Coord. Chem. Rev.* **1994**, *130*, 509−621.
(30) Steigerwald, M. L.; Siegrist, T.; Gyorgy, E. M.; Hessen, B.; Kwon, Y. U.; Tanzler, S. M. Effect of Diverse Ligands on the Course of a Molecules-to-Solids Process and Properties of Its Intermediates. *Inorg. Chem.* **1994**, *33*, 3389−3395.
(31) Lever, A. B. P. Electrochemical Parametrization of Metal Complex Redox Potentials, Using the Ruthenium(III)/Ruthenium-(II) Couple to Generate a Ligand Electrochemical Series. *Inorg. Chem.* **1990**, *29*, 1271−1285.
(32) Chatt, J.; Kan, C. T.; Leigh, G. J.; Pickett, C. J.; Stanley, D. R. Transition-Metal Binding Sites and Ligand Parameters. *J. Chem. Soc., Dalton Trans.* **1980**, 2032−2038.
(33) Banda, R. M. H.; Dance, I. G.; Bailey, T. D.; Craig, D. C.; Scudder, M. L. Cadmium Polysulfide Complexes, $[Cd(S_x)(S_y)]^{2-}$: Syntheses, Crystal and Molecular Structures, and ^{113}Cd NMR Studies. *Inorg. Chem.* **1989**, *28*, 1862−1871.
(34) Bailey, T. D.; Banda, R. M. H.; Craig, D. C.; Dance, I. G.; Ma, I. N. L.; Scudder, M. L. Mercury Polysulfide Complexes, $[Hg(S_x)(S_y)]^{2-}$: Syntheses, ^{199}Hg NMR Studies in Solution, and Crystal Structure of $(Ph_4P)_4[Hg(S_4)_2]Br_2$. *Inorg. Chem.* **1991**, *30*, 187−191.

https://doi.org/10.1021/acs.inorgchem.2c00684
Inorg. Chem. 2022, 61, 8241−8249